Journal of Applied Physics

Gate-tunable modulation of the optical properties of multilayer graphene by the reversible intercalation of ionic liquid anions

Cite as: J. Appl. Phys. **132**, 095102 (2022); https://doi.org/10.1063/5.0093651
Submitted: 29 March 2022 • Accepted: 15 July 2022 • Published Online: 06 September 2022

Zhi Cai, Indu Aravind, Haley Weinstein, et al.

Journal of Applied Physics | ARTICLE | scitation.org/journal/jap

Gate-tunable modulation of the optical properties of multilayer graphene by the reversible intercalation of ionic liquid anions

Cite as: J. Appl. Phys. **132**, 095102 (2022); doi: 10.1063/5.0093651
Submitted: 29 March 2022 · Accepted: 15 July 2022 ·
Published Online: 6 September 2022

Zhi Cai,[1] Indu Aravind,[2] Haley Weinstein,[3] Ruoxi Li,[1] Jiangbin Wu,[3] Han Wang,[1,3,4] Jonathan Habif,[3,5] and Stephen B. Cronin[2,3,4,a)]

AFFILIATIONS

[1]Mork Family Department of Chemical Engineering and Materials Science, University of Southern California, Los Angeles, California 90089, USA
[2]Department of Physics and Astronomy, University of Southern California, Los Angeles, California 90089, USA
[3]Ming Hsieh Department of Electrical Engineering, University of Southern California, Los Angeles, California 90089, USA
[4]Department of Chemistry, University of Southern California, Los Angeles, California 90089, USA
[5]Information Sciences Institute, University of Southern California, Waltham, Massachusetts 02451, USA

[a)]**Author to whom correspondence should be addressed:** scronin@usc.edu

ABSTRACT

We demonstrate a substantial modulation of the optical properties of multilayer graphene (~100 layers) using a simple device consisting of a multilayer graphene/polymer electrolyte membrane/gold film stack. Applying a voltage of 3–4 V drives the intercalation of anion $[TFSI]^-$ [ion liquid diethylmethyl(2-methoxyethyl)ammonium bis(trifluoromethylsulfonyl)imide [DEME][TFSI]] resulting in the reversible modulation of the properties of this optically dense material. Upon intercalation, we observe an abrupt shift of 35 cm^{-1} in the *G* band Raman mode, an abrupt increase in FTIR reflectance over the wavelength range from 1.67 to 5 μm (2000–6000 cm^{-1}), and an abrupt increase in luminescent background observed in the Raman spectra of graphene. All of these abrupt changes in the optical properties of this material arise from the intercalation of the $TFSI^-$ ion and the associated change in the free carrier density ($\Delta n = 10^{20}$ cm^{-3}). Suppression of the 2D band Raman mode observed around 3 V corresponds to Pauli blocking of the double resonance Raman process and indicates a modulation of the Fermi energy of $\Delta E_F = 1.1$ eV.

I. INTRODUCTION

Over the past 15 years, there has been a large amount of research on various forms of graphene.[1,2] Highlights of this research include the observation of the quantum hall effect,[3] high thermal conductivity,[4,5] ultrahigh electron mobilities,[6] transparent conducting electrodes,[7] tunable plasmon-polaritons,[8] and superconducting phases of graphene.[9] In addition to these fundamental phenomena, the wide tunability of graphene's properties with electrostatic and electrochemical doping gives rise to many practical applications.[10,11]

The properties of bulk graphite have been exploited since the 1980s as anode materials for Li ion batteries[12] and high strength-to-weight ratio composite materials,[13] and a large amount of research has been conducted on graphite intercalation compounds (GICs).[14,15] Currently, the main application of graphite is in rechargeable lithium ion batteries. For example, electric vehicles typically contain 83 kg of graphite as the anode material, in which lithium ions intercalate between the layers enabling extremely high charge storage capacities up to 372 mAh/g. This property of graphite is a direct result of its layered structure, which enables the intercalation between the weakly bound layers that are held together by van der Waals forces.

Bao *et al.* studied intercalation-induced transparency in graphitic materials using Li ion intercalation in the visible range.[16] They introduced a Drude model with interband transitions to explain the basic mechanism of Pauli blocking. The Raman spectra of graphite intercalation compounds was reported by Chacon-Torres.[17] These spectra reveal the staging of potassium intercalation and the associated strain induced in the lattice that is associated with intercalation. More recently, in the works of Salihoglu *et al.*[18] and Ergoktas *et al.*,[19]

multilayer graphene (MLG) grown by chemical vapor deposition (CVD) was used in conjunction with an ionic liquid electrolyte to demonstrate controllable infrared and thermal signatures.

II. EXPERIMENTS AND RESULTS

Figure 1 shows an illustration and cross-sectional diagram of the multilayer graphene device. Multilayer graphene is grown by chemical vapor deposition (CVD) on a 0.125 mm thick nickel foil (Sigma-Aldrich #7440-02-0). The growth temperature is 1000 °C, the flow rates are 100 SCCM of H_2 and 30 SCCM of CH_4 for 20 min, and the pressure in the chamber was approximately 10 Torr. After growth, we etch the nickel foil with nickel etchant (Transene Company, Inc. Nickel Etchant Type I). After the etching process, the multilayer graphene (MLG), which is hydrophobic, floats on top of the nickel etchant. We then transfer the MLG to a solution of DI water to remove any residual ions from the nickel etchant. Then, we immerse the porous polyethersulfone (PES) membrane [Membrane Solutions (Nantong) Co., Ltd., #MSPES260120] into the DI water solution and transfer the MLG onto the membrane. Our device, consisting of multilayer graphene (MLG) (approximately $1.5 \times 1.5\,\text{cm}^2$, 30 nm thick), deposited on the PES membrane (approximately $2 \times 2\,\text{cm}^2$, 1 μm thick), which is then deposited onto a gold electrode ($2.54 \times 2.54\,\text{cm}^2$, 100 nm thick), as shown in Fig. S1 in the supplementary material. The thickness of the MLG is determined by Raman spectroscopy, as shown in Fig. S2 in the supplementary material. An atomic force microscope (AFM) image of the MLG device is shown in Fig. S3 in the supplementary material, which has a roughness of approximately 10 nm as can be seen in cross-sectional plots. However, before depositing on the Au electrode, an ionic liquid diethylmethyl(2-methoxyethyl)ammonium bis(trifluoromethylsulfonyl) imide ([DEME][TFSI]) is used to fill the interstitial spaces in the polyelectrolyte membrane enabling a voltage to be applied between the bottom Au electrode and the multilayer graphene top electrode, which results in reversible intercalation of $[\text{TFSI}]^-$ anions.

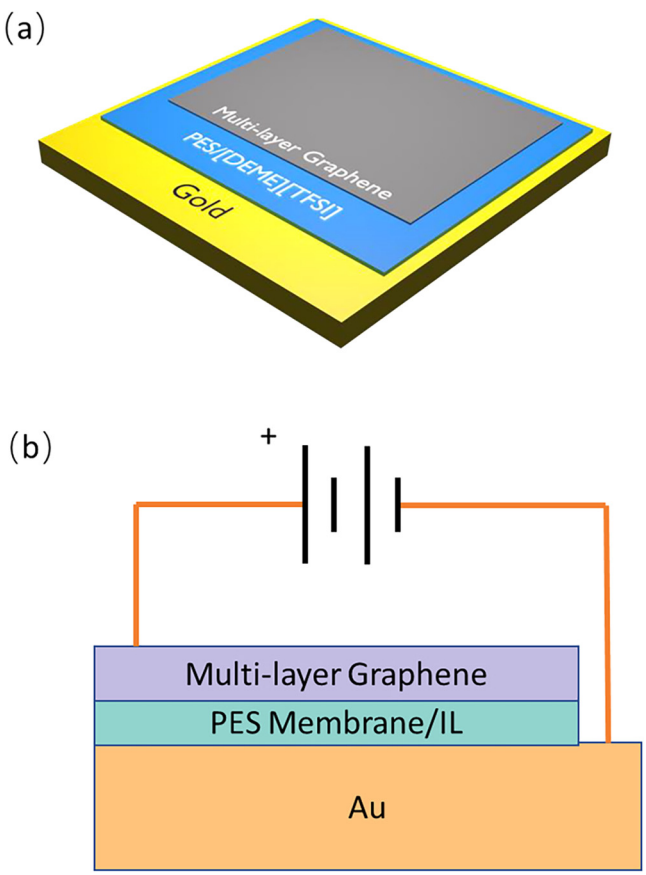

FIG. 1. (a) Schematic diagram and (b) cross-sectional diagram of the sample consisting of a multiple layer graphene top electrode, porous PES membrane filled with ionic liquid ([DEME][TFSI]), and the gold electrode bottom contact.

We measured the Raman spectra of MLG devices at various voltages between 0 and 4 V, as plotted in Fig. 2(a). Here, the incident laser wavelength is 532 nm, and the laser spot size is approximately 1 μm in diameter. Over the range from 1200 to 1700 cm^{-1}, we observe the D band (1350 cm^{-1}), G band (1582 cm^{-1}), and intercalated G band (i.e., G_{int} band) (1620 cm^{-1}). After performing Raman spectroscopy, a comparable device is tested using a mirror-based Hyperion microscope coupled to a Bruker FTIR spectrometer. The reflectance of the device is measured under the same range of voltages as in Raman spectroscopy measurements. Here, the spot size of the infrared light is $100 \times 100\,\mu\text{m}^2$, and the wavelength range extends from 1.67 to 5 μm (i.e., 2000 to 6000 cm^{-1}).

Figure 2(a) shows a waterfall plot of the Raman spectra taken at various voltages between 0 and 4 V. Here, we see the abrupt onset of the intercalated G band (i.e., G_{int}) at 1620 cm^{-1} at 3.5 V, corresponding to the intercalated state of graphene. It is somewhat surprising that these large anions (i.e., $[\text{TFSI}]^-$) can intercalate between the layers of the graphene so effectively. Nevertheless, this abrupt shift in the G band is a well-known signature of intercalation and stands in contrast to electrochemical doping, wherein the frequency of the G band increases monotonically as a function of the applied voltage. Figure 2(b) shows a corresponding series of FTIR spectra taken from a comparable device. Here, we see a large increase in reflectance by a factor of 100% over the 2000–6000 cm^{-1} range. This change in reflectance occurs because of the large increase in the free carrier concentration from approximately 10^{18} to $10^{20}\,\text{cm}^{-3}$ over this applied voltage range. Here, the device becomes more reflective (i.e., less absorbtive) under the applied potential, as the heavily doped graphite undergoes Pauli blocking at these wavelengths due to the large increase in Fermi energy. At large applied potentials, we begin to see suppression of the 2D-band Raman mode due to Pauli blocking of the double resonance Raman process (illustrated in Fig. S4 in the supplementary material), which occurs at $|\Delta E_F| > 1/2E_{ex}$, where $E_{ex} = 2.33$ eV. For graphene, we can calculate the carrier density by $\Delta n = \left(\frac{E_F}{\hbar v_F}\right)^2/\pi$, where v_F is the graphene Fermi velocity and $\hbar$ is the reduced Planck constant, yielding $\Delta n = 2.2 \times 10^{21}\,\text{cm}^{-3}$.[20] In addition, we observe the emergence of four voltage-dependent dips in the FTIR spectra at 2106, 2381, 4085, and 4409 cm^{-1}. While we do not fully understand the origin of these peaks, one possibility is that they are

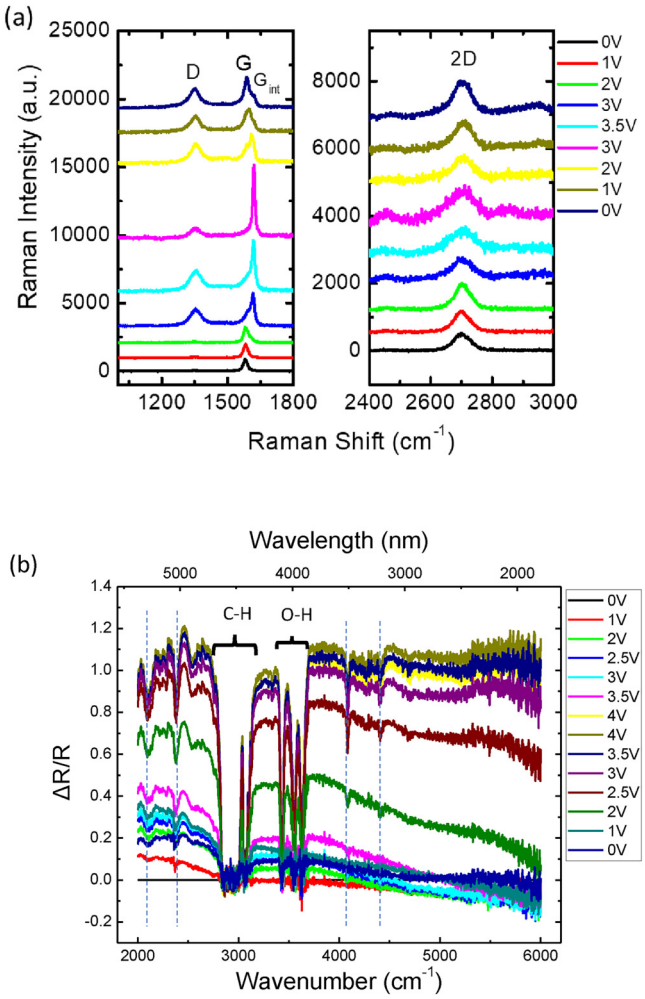

FIG. 2. (a) Waterfall plot of the voltage-dependent Raman spectra (background subtracted). (b) Differential infrared reflectance spectra under various applied voltages.

due to the S–N–S and CF_3 stretch frequencies of the $[TFSI]^-$ anions and their higher order harmonics.[21] Another possibility is that they originate from the formation of graphene oxide; however, this is unlikely since such oxidation would not be reversible.[22]

Figure 3 shows the voltage-dependent plots summarizing the key features in Raman and FTIR spectra over the 0–4 V range. Figure 3(a) shows the G_{int}/G band intensity ratio plotted as a function of applied voltage. Above 3 V, we observe an abrupt onset of the G_{int} band at 1620 cm^{-1}, corresponding to the intercalated state of graphite. Figure 3(b) shows the luminescent background observed in the Raman spectra at 2250 cm^{-1} plotted as a function of the applied voltage (see Fig. S5 in the supplementary material for the Raman Spectra exhibiting this luminescent background). Here, we observe an abrupt increase in the luminescent background intensity on the order of 10× around 3 V, which is due to the large

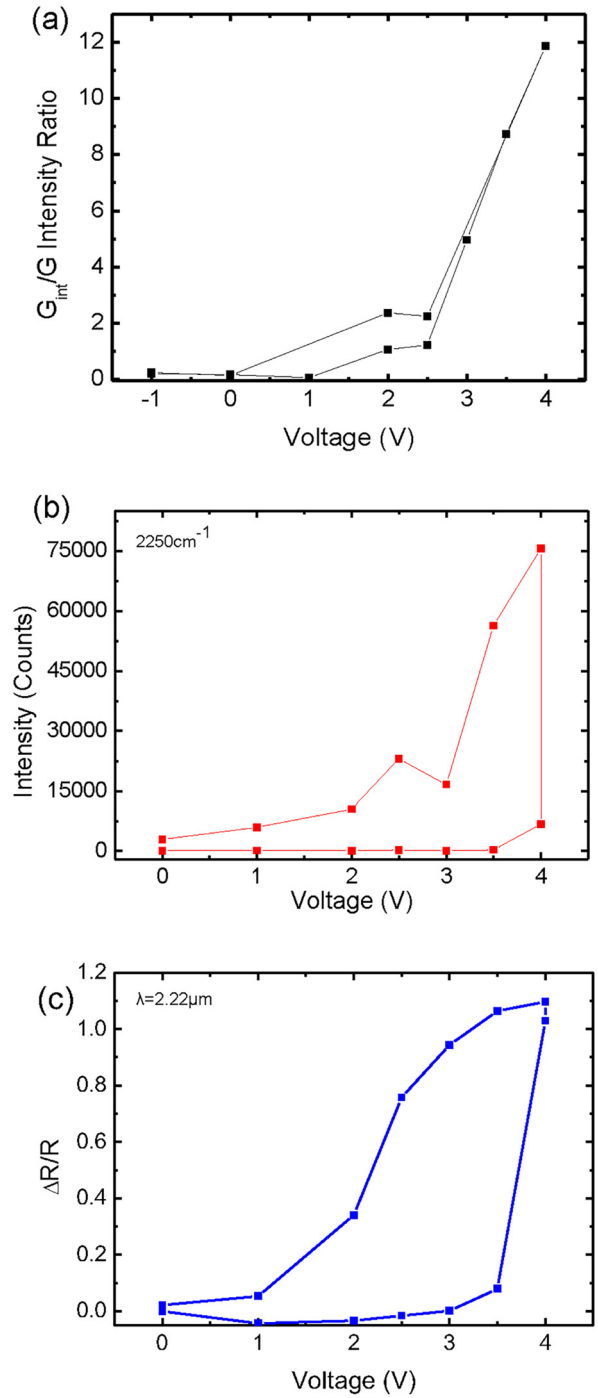

FIG. 3. (a) Raman intensity ratio between the intercalated G_{int} band (1620 cm^{-1}) and the uncharged G band (1585 cm^{-1}) under various applied voltages. (b) Luminescent background intensity observed in the Raman spectra at 2250 cm^{-1} under various applied voltages. (c) Differential FTIR reflectance observed at 2.22 μm under various applied voltages relative to the reflectance at zero applied voltage.

increase in free carrier density. A similar luminescent background is seen in the Raman spectra of strongly plasmon of metals, including gold, silver, and copper. Figure 3(c) shows the FTIR reflectance at 4500 cm^{-1} (i.e., $\lambda = 2.22\,\mu m$), which exhibits a similar voltage-dependent profile to that of the Raman spectra. In addition, Figs. 3(b) and 3(c) exhibit hysteresis that are due to the relatively slow intercalation/de-intercalation dynamics, as limited by the diffusion of the relatively large anions (radius = 0.9 nm). These hysteresis can be either an advantage or a disadvantage from a device application point of view. For telecommunication applications, it is desirable to cycle at high frequencies. For filters and modulators, the hysteresis can enable low-power switching between the intercalation states (intercalated/de-intercalated) using voltage pulses without constantly applying a voltage (low power consumption). The time constants for intercalation of our devices are around $\tau = 38$ and 63 ms for de-intercalation, as plotted in Fig. S6 in the supplementary material. However, it is possible to increase the de-intercalation dynamics by increasing the temperature and bias conditions. That is, the hysteresis can potentially be tuned by varying temperature. It is worth mentioning that this intercalation process is not totally reversible. As noted in the Raman spectra, a relatively large D-band persists after the first intercalation process. Nevertheless, the IR absorption, G_{int}/G band intensity ratio, and the plasmon can background intensity drop back to their pre-intercalation values. Therefore, from the device performance perspective, this intercalation process is effectively reversible. In addition, we observe an irreversible change in the D band Raman intensity after the first intercalation cycle. The D band originates from sp^3 hybridization and defects (i.e., broken sp^2 symmetry), which can occur upon intercalation.[23] The irreversibility of this feature indicates that there are defects created under these high anodizing potentials. In addition, the size of the $[TFSI]^-$ ion is approximately 7 Å, which is 2.8 times the graphene lattice constant (i.e., 2.46 Å) and 2 times of the interlayer distance of MLG (i.e., 3.5 Å). Thus, during the intercalation process, defects are induced in the graphene crystal structure. Despite these defects, the intercalation/deintercalation process seems to continue reversibly after many cycles, as demonstrated in Fig. S6 in the supplementary material.

Figure 4 shows a parametric plot of the change in FTIR reflectance plotted as a function of the luminescent background intensity observed in the Raman spectra over this 0–4 V range of applied potentials. This figure shows that there is indeed a strong correlation between these two properties. Both arise from a large increase in the free carrier density of this material, which changes the IR reflectance due to Pauli blocking and an associated gate voltage-induced transparency in this wavelength range. The luminescent background in the Raman spectra arises from inelastic scattering via free-carrier decay pathways.

In conclusion, we have observed a wide modulation in the optoelectronic properties of multilayer graphene in the infrared and visible wavelength range. The abrupt changes observed are the result of intercalation of ions in a non-aqueous electrolyte, which results in strong doping of the material. The large increase in free carrier density is observed through the emergence of a blue-shifted G band Raman frequency (i.e., G_{int}), a luminescent background in the Raman spectra, and an abrupt change in the infrared reflectance that occurs around 3 V of applied potential. In contrast to studies of monolayer graphene, which have exemplified electrostatic and electrochemical tunability, these results demonstrate the widely tunable properties in an optically dense material, which is suitable for practical applications. We believe that this fundamental mechanism will enable active optoelectronics in the infrared wavelength range, where such devices are currently lacking.

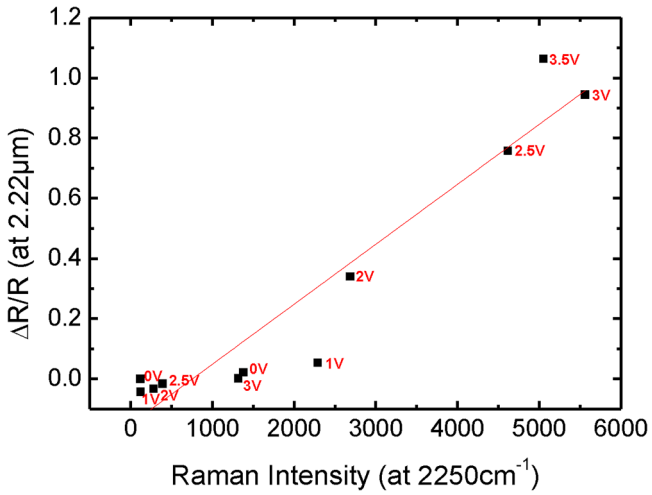

FIG. 4. Linear fit to the background Raman intensity (at 2550 cm^{-1}) and FTIR reflection (at 2.22 μm).

SUPPLEMENTARY MATERIAL

See the supplementary material for a photograph of the device, MLG thickness determination, AFM image of the device, illustration of the Pauli blocking process for the 2D band Raman mode, raw data plot of the voltage-dependent Raman spectra, and time-resolved temperature measurements.

ACKNOWLEDGMENTS

This research was supported by the U.S. Department of Energy, Office of Basic Energy Sciences under Award No. DE-FG02-0746376 (Z.C.), the Army Research Office (ARO) under Award No. W911NF-19-1-0257 (R.L.) and under Grant No. W911NF-19-1-0111, the National Science Foundation (NSF) under Award No. CBET-2012845 (H.W.), and The Air Force Office of Scientific Research (AFOSR) under Grant No. FA9550-19-1-0115 (I.A.).

AUTHOR DECLARATIONS

Conflict of Interest

The authors declare no conflicts of interest.

Author Contributions

Zhi Cai: Conceptualization (equal); Data curation (lead); Formal analysis (lead); Validation (lead); Writing – original draft (lead); Writing – review and editing (equal). **Indu Aravind:** Data curation (equal); Validation (equal). **Haley Weinstein:** Data curation (equal); Validation (equal). **Ruoxi Li:** Data curation (supporting). **Jiangbin Wu:** Data curation (supporting). **Han Wang:** Data curation (supporting). **Jonathan Habif:** Data curation (supporting). **Stephen B. Cronin:** Conceptualization (lead); Funding acquisition (lead); Methodology (equal); Project administration (lead); Supervision (lead); Writing – original draft (equal); Writing – review and editing (equal). **Stephen B. Cronin:** Conceptualization (lead); Funding acquisition (lead); Methodology (equal); Project administration (lead); Supervision (lead); Writing – original draft (equal); Writing – review and editing (equal).

DATA AVAILABILITY

The data that supports the findings of this study are available within the article and its supplementary material.

REFERENCES

[1]K. S. Novoselov, A. K. Geim, S. V. Morozov, D. Jiang, Y. Zhang, S. V. Dubonos, I. V. Grigorieva, and A. A. Firsov, "Electric field effect in atomically thin carbon films," Science **306**, 666–669 (2004).

[2]A. K. Geim and K. S. Novoselov, "The rise of graphene," Nat. Mater. **6**, 183–191 (2007).

[3]Y. B. Zhang, Y. W. Tan, H. L. Stormer, and P. Kim, "Experimental observation of the quantum Hall effect and berry's phase in graphene," Nature **438**, 201–204 (2005).

[4]A. A. Balandin, S. Ghosh, W. Z. Bao, I. Calizo, D. Teweldebrhan, F. Miao, and C. N. Lau, "Superior thermal conductivity of single-layer graphene," Nano Lett. **8**, 902–907 (2008).

[5]J. Yang, E. Ziade, C. Maragliano, R. Crowder, X. Wang, M. Stefancich, M. Chiesa, A. K. Swan, and A. J. Schmidt, "Thermal conductance imaging of graphene contacts," J. Appl. Phys. **116**, 023515 (2014).

[6]K. I. Bolotin, K. J. Sikes, Z. Jiang, M. Klima, G. Fudenberg, J. Hone, P. Kim, and H. L. Stormer, "Ultrahigh electron mobility in suspended graphene," Solid State Commun. **146**, 351–355 (2008).

[7]R. R. Nair, P. Blake, A. N. Grigorenko, K. S. Novoselov, T. J. Booth, T. Stauber, N. M. R. Peres, and A. K. Geim, "Fine structure constant defines visual transparency of graphene," Science **320**, 1308 (2008).

[8]J. N. Chen, M. Badioli, P. Alonso-Gonzalez, S. Thongrattanasiri, F. Huth, J. Osmond, M. Spasenovic, A. Centeno, A. Pesquera, P. Godignon, A. Z. Elorza, N. Camara, F. J. G. de Abajo, R. Hillenbrand, and F. H. L. Koppens, "Optical nano-imaging of gate-tunable graphene plasmons," Nature **487**, 77–81 (2012).

[9]B. Uchoa and A. H. C. Neto, "Superconducting states of pure and doped graphene," Phys. Rev. Lett. **98**, 146801 (2007).

[10]M. Kim, N. S. Safron, C. Huang, M. S. Arnold, and P. Gopalan, "Light-driven reversible modulation of doping in graphene," Nano Lett. **12**, 182–187 (2012).

[11]P. L. Levesque, S. S. Sabri, C. M. Aguirre, J. Guillemette, M. Siaj, P. Desjardins, T. Szkopek, and R. Martel, "Probing charge transfer at surfaces using graphene transistors," Nano Lett. **11**, 132–137 (2011).

[12]P. Schoderbock and H. P. Boehm, "Observations of staging in the electrochemical intercalation of lithium into graphite from dimethyl-sulfoxide solutions," Synth. Met. **44**, 239–246 (1991).

[13]F. Chipps and B. M. Vanderbilt, "Graphite composites-hight-strength-thermosets from synthetic elastomers," in Elastomerics (1983), Vol. 115, p. 37.

[14]M. S. Dresselhaus and G. Dresselhaus, "Intercalation compounds of graphite," Adv. Phys. **30**, 139–326 (1981).

[15]A. P. Crary, "Thermal conductivity of acheson graphite," Physics **4**, 332–333 (1933).

[16]W. Z. Bao, J. Y. Wan, X. G. Han, X. H. Cai, H. L. Zhu, D. H. Kim, D. K. Ma, Y. L. Xu, J. N. Munday, H. D. Drew, M. S. Fuhrer, and L. B. Hu, "Approaching the limits of transparency and conductivity in graphitic materials through lithium intercalation," Nat. Commun. **5**, 1–9 (2014).

[17]J. C. Chacon-Torres, L. Wirtz, and T. Pichler, "Manifestation of charged and strained graphene layers in the Raman response of graphite intercalation compounds," ACS Nano **7**, 9249–9259 (2013).

[18]O. Salihoglu, H. B. Uzlu, O. Yakar, S. Aas, O. Balci, N. Kakenov, S. Balci, S. Olcum, S. Suzer, and C. Kocabas, "Graphene-based adaptive thermal camouflage," Nano Lett. **18**, 4541–4548 (2018).

[19]M. S. Ergoktas, G. Bakan, P. Steiner, C. Bartlam, Y. Malevich, E. Ozden-Yenigun, G. L. He, N. Karim, P. Cataldi, M. A. Bissett, I. A. Kinloch, K. S. Novoselov, and C. Kocabas, "Graphene-enabled adaptive infrared textiles," Nano Lett. **20**, 5346–5352 (2020).

[20]S. Das Sarma, S. Adam, E. H. Hwang, and E. Rossi, "Electronic transport in two-dimensional graphene," Rev. Mod. Phys. **83**, 407–470 (2011).

[21]G. Hu, R. S. Anaredy, M. Alamri, Q. Liu, G. P. Pandey, C. Ma, M. Liu, S. K. Shaw, J. Li, and J. Z. Wu, "Probing the relationship of cations-graphene interaction strength with self-organization behaviors of the anions at the interface between graphene and ionic liquids," Appl. Surf. Sci. **479**, 576–581 (2019).

[22]V. Ţucureanu, A. Matei, and A. M. Avram, "FTIR spectroscopy for carbon family study," Crit. Rev. Anal. Chem. **46**, 502–520 (2016).

[23]A. Ferrari, J. Robertson, S. Reich, and C. Thomsen, "Raman spectroscopy of graphite," Philos. Trans. Royal Soc. A **362**, 2271–2288 (2004).